Electronic Supplementary Material (ESI) for Inorganic Chemistry Frontiers.

Supporting Information

In-situ implanting MnO nanoparticles into nanorod-assembled carbon microspheres enables performance-enhanced room-temperature Na-S batteries

Xiang Long Huang,[1] Pan Xiang,[1] Hanwen Liu,[3] Chi Feng,[1] Shaohui Zhang,[4] Ziqi Tian,[5] Hua Kun Liu,[2] Shi Xue Dou,[2]* Zhiming Wang[1]*

[1] Institute of Fundamental and Frontier Sciences, University of Electronic Science and Technology of China, 610054, P. R. China
E-mail: zhmwang@uestc.edu.cn

[2] Institute for Superconducting and Electronic Materials, University of Wollongong, NSW
E-mail: shi@uow.edu.au

[3] School of Chemical Engineering, The University of Queensland, St. Lucia, Brisbane, QLD 4072, Australia

[4] Guangdong Provincial Key Laboratory of Micro/Nano Optomechatronic Engineering, College of Mechatronics and Control Engineering, Shenzhen University, Shenzhen 518060, P. R. China

[5] Ningbo Institute of Materials Technology and Engineering, Chinese Academy of Sciences, Ningbo, 315201 P. R. China

Preparation of precursor

The precursor was synthesized via a simple self-assembly process at an ambient condition. Firstly, 980 mg of manganese acetate tetrahydrate and 4g of polyvinylpyrrolidone (PVP, Mw=58000) were completely dissolved into a mixed solution of alcohol and distilled water with a volume ratio of 3:1 (solution I), and 1800 mg of 1, 3, 5-benzenetricarboxylic acid was completely dissolved into a mixed solution of alcohol and distilled water with a volume ratio of 2:1 (solution II). Then, solution II was directly poured into solution I, violently stirred for half hour, and stood overnight. Afterwards, the as-produced cloudy solution was separated via a vacuum filtration, rinsed with alcohol for three times, and dried for 12 hours at 60℃ in a drying oven. Finally, the resulting white powder was Mn-MOF.

Preparation of MnO@NACM and NACM

The as-obtained Mn-MOF was carbonized at 800℃ for 3 hours under the protection of uniform argon flow to generate a hybrid of MnO and carbon (marked as MnO-C), accompanied with a yield of about 50%. The MnO-C hybrid was soaked in a dilute H_2SO_4 solution for several hours to remove partial MnO (labelled as MnO@NACM). After MnO was fully removed, the residual was pure porous carbon (NACM).

Preparation of S/MnO@NACM and S/NACM composites

The MnO@NACM and S powder with a mass ratio of 55:45 were uniformly mixed and further annealed at 155 °C for 12 hours to produce the S/MnO@NACM composite. The S/NACM composite was obtained via the same method, using the control sample NACM.

Materials characterization

The morphologies and nanostructures of all the material samples observed via field emission scanning electron microscope (ZEISS, GeminiSEM 300) and transition electron microscope (Tecnai G2 F20 S-TWIN). The elemental distributions of the S/MnO@NACM and S/NACM composites composite were collected by energy

dispersive spectrometry (EDS). The crystal structures and chemical states of all the samples were analyzed employing an X-ray diffractometer (XRD) with Cu K-alpha radiation and X-ray photoelectron spectra (XPS, Thermo Scientific ESCALAB 250Xi), respectively. Raman patterns of all the samples were acquired via InviaRefl (Renishaw, UK) with 532 nm laser light. The specific surface areas and pore distributions of samples were investigated by Brunauer-Emmett-Teller method (BSD PS2, China). The contents of MnO and S in the samples were estimated using thermogravimetric analysis (TG 209, Germany) at corresponding gas atmosphere.

Adsorption experiment

The sublimed S powder and anhydrous sodium sulfide (Na_2S) powder with a molar ratio of 5:1 were dissolved into TEGDME solvent and stirred overnight in an argon-filled glovebox to produce a blackish green Na_2S_6 solution. The solution was then diluted to a low concentration for the adsorption test. Then, an identical weight of NACM and MnO@NACM composite were added into the low-concentration Na_2S_6 solutions with the same volume to observe and compare the color change of target solution. Finally, ultraviolet-visible (UV) absorption spectra of target solutions were examined after soaking the samples in the Na_2S_6 solution for 12 h to carry out comparison.

Coin-cell assembly and electrochemical measurement

The S/MnO@NACM composite, Ketjen black, and PVDF were mixed at a mass ratio of 8:1:1 in NMP solvent and grinded to a homogeneous slurry. The slurry was uniformly casted on a carbon-coated aluminum foil current collector, dried at 80°C for 12 hours in a vacuum oven to volatilize NMP, and finally cut into disk electrodes with a diameter of 12 mm. The loading content of S in every electrode is 0.8-1.0 mg. For performance evaluation, these disks were used to assemble 2032-type coin cells in an argon-filled glove box (oxygen content < 0.01 ppm; water content < 0.01 ppm). Sodium foils with a diameter of 15.6 mm and a thickness of 500 μm and glass fiber disc (Whatman, GF1820-125) with a diameter of 19 mm served as the counter electrodes

and separators, separately. The electrolyte is 1M $NaClO_4$ dissolved into mixture solvent of EC and PC with 5% of FEC as an additive. The amount of electrolyte in every coin cell is 55 μL. The galvanostatic discharge-charge tests were conducted on a LAND instrument testing system under a room temperature (25 °C ± 3 °C), using a voltage window of 0.8-2.8 V. CV curves were recorded on electrochemical workstation (Chenhua Instrument, CHI 660E) and EIS was also carried out on electrochemical workstation (Chenhua Instrument, CHI 660E) with a frequency range from 0.01 Hz to 100 kHz.

Theoretical calculations

All theoretical calculations based on the density functional theory were performed by the Vienna ab initio Simulation Package by utilizing the generalized gradient approximation of Perdew-Burke-Ernzerhof with Grimme dispersion correction. The cut-off energy of the plane-wave basis was set to 520 eV and the projector augmented wave pseudopotentials were used. A 0.04 1/Å separation was applied to the k-points and a smearing of 0.05 eV was used. The atomic positions were optimized by the Broyden-Fletcher-Goldfarb-Shannon algorithm until the maximum force converged to 0.02 eV/Å. DFT+U method was applied with Ueff of Mn equal to 3.9 eV. The interaction strength between Na_2S_6 and substrates were evaluated using E_{ad} defined as:

$$E_{ad} = E_{total} - E_{sub} - E_{Na2S6}$$

where E_{total} and E_{sub} indicate the energy of substrates with and without the Na_2S_6 adsorption respectively, and E_{Na2S6} denotes the energy of isolated Na_2S_6 clusters.

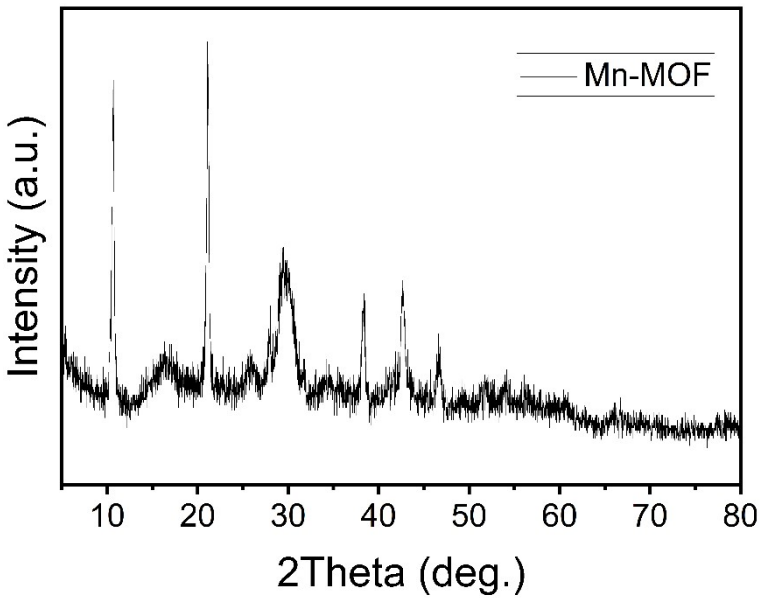

Figure S1. XRD pattern of the Mn-MOF.

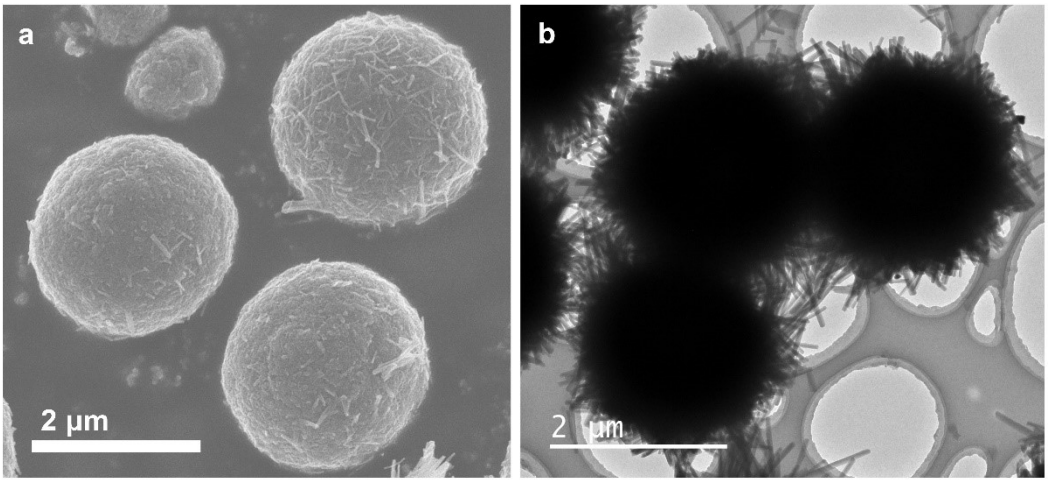

Figure S2. (a) FESEM image (b) and TEM image (b) of the Mn-MOF precursor.

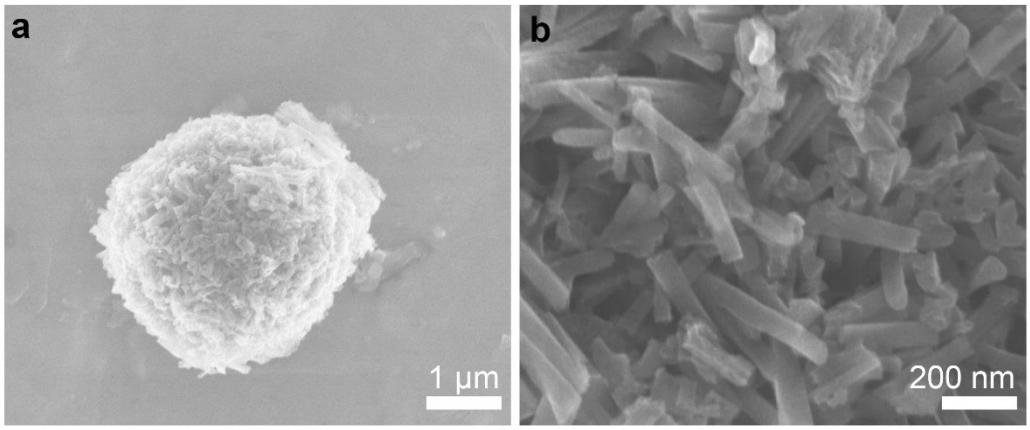

Figure S3. (a-b) FESEM images of the MnO@NACM composite.

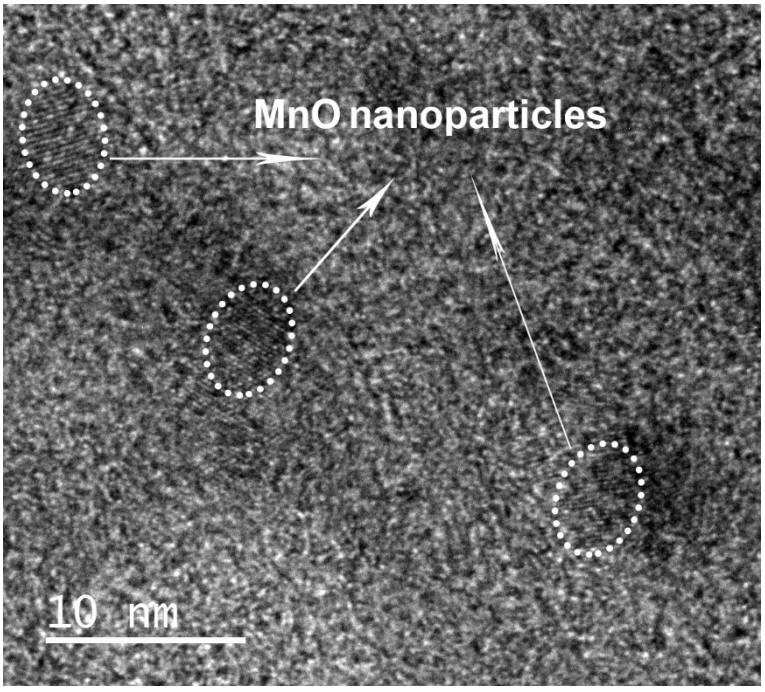

Figure S4. HRTEM image of the MnO@NACM composite.

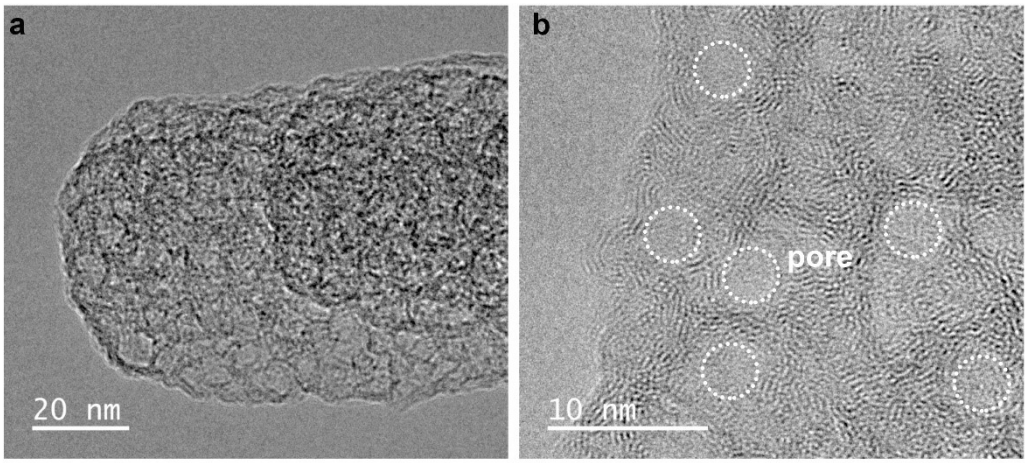

Figure S5. HRTEM images of the MnO@NACM composite.

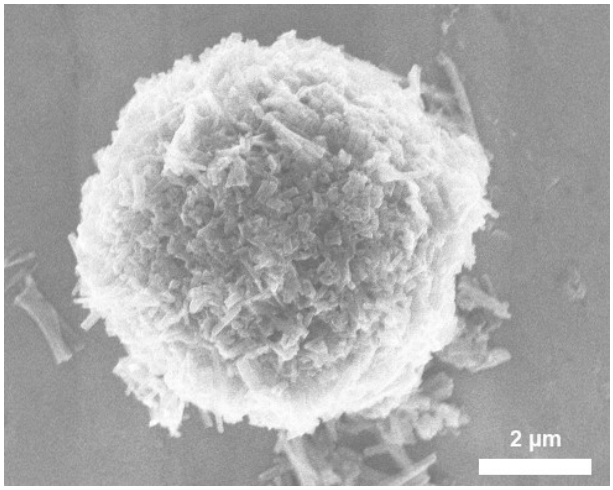

Figure S6. FESEM image of the S/MnO@NACM composite.

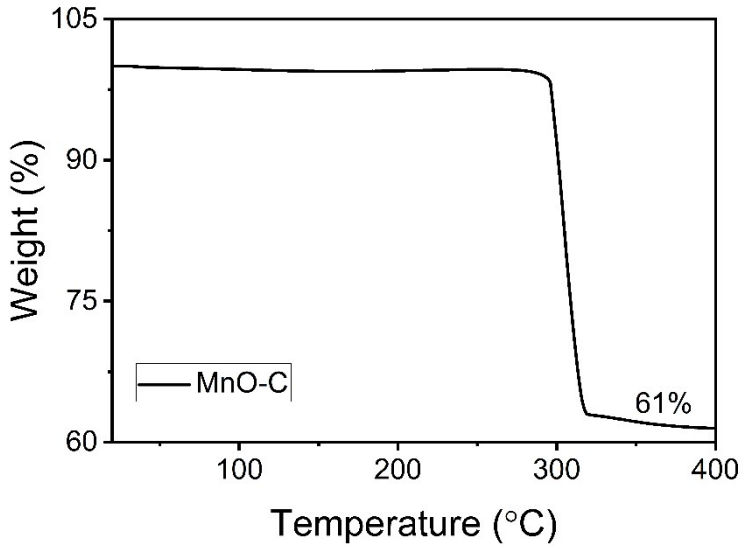

Figure S7. TGA curve of the MnO-C hybrid at oxygen atmosphere.

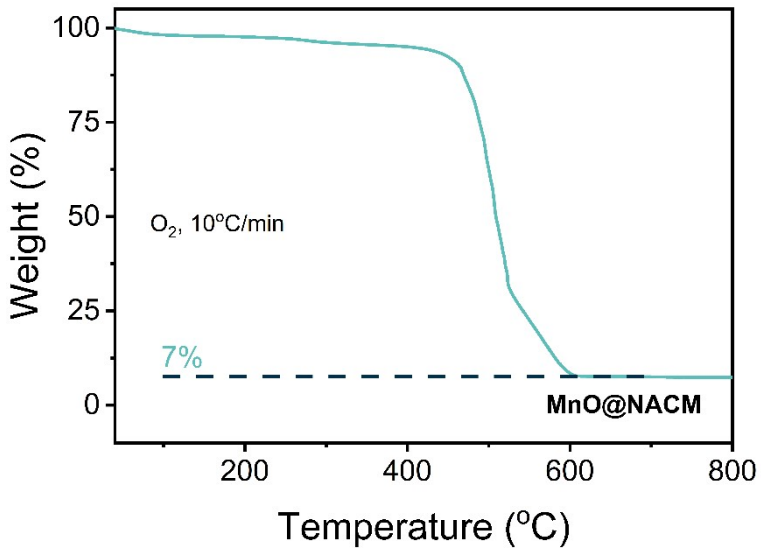

Figure S8. TGA curve of the MnO@NACM at oxygen atmosphere.

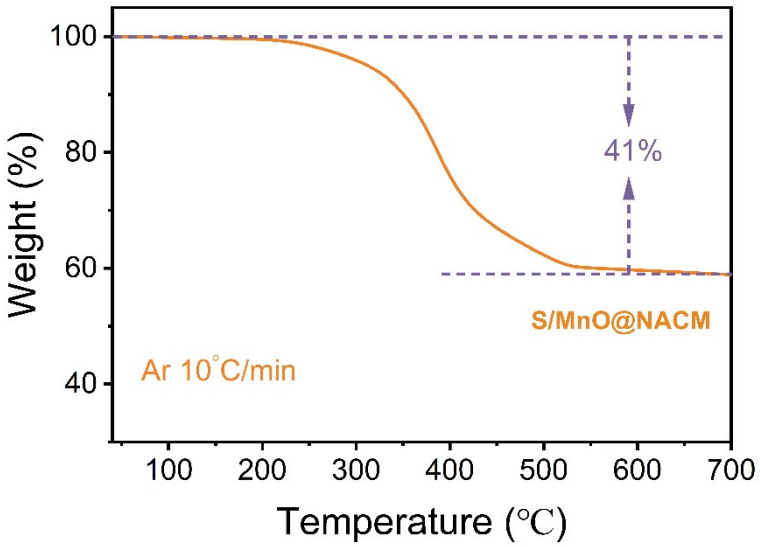

Figure S9. TGA curve of the S/MnO@NACM composite at Ar atmosphere.

Table S1. A summary of pore volume and surface area of the samples.

Sample	**Pore volume (cm^{-3} g^{-1})**	**Surface area (m^{-2} g^{-1})**
MnO@NACM	0.913	683.4
S/MnO@NACM	0.348	54.9

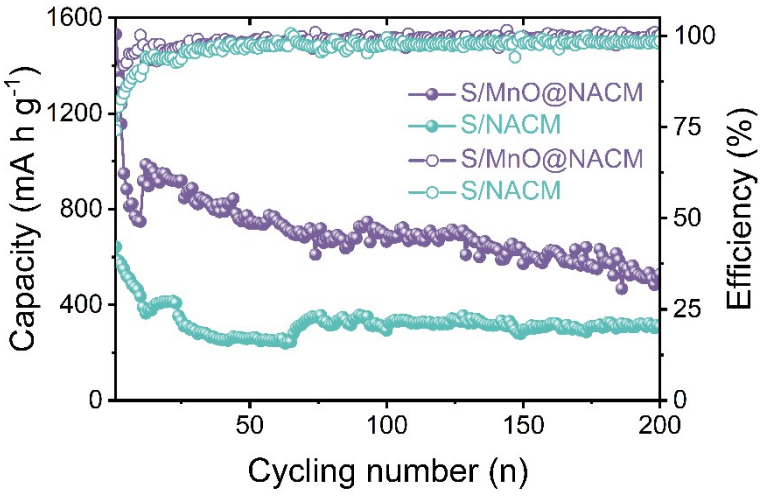

Figure S10. Cycling performance of the Na-S coin cells at 0.1 A g^{-1}.

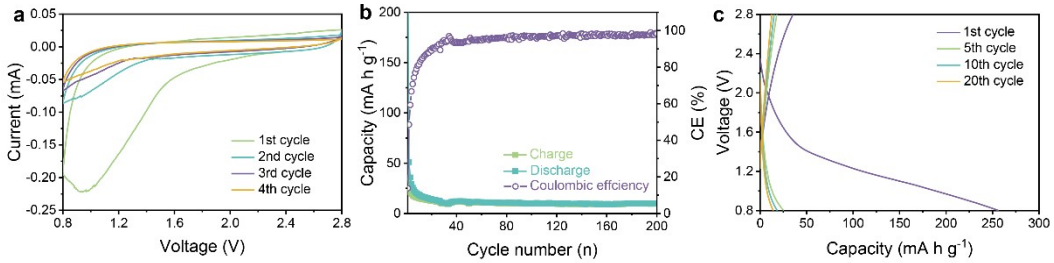

Figure S11. CV curves (a), cycling performance (b), discharge-charge profiles (c) of the MnO@NACM composite.

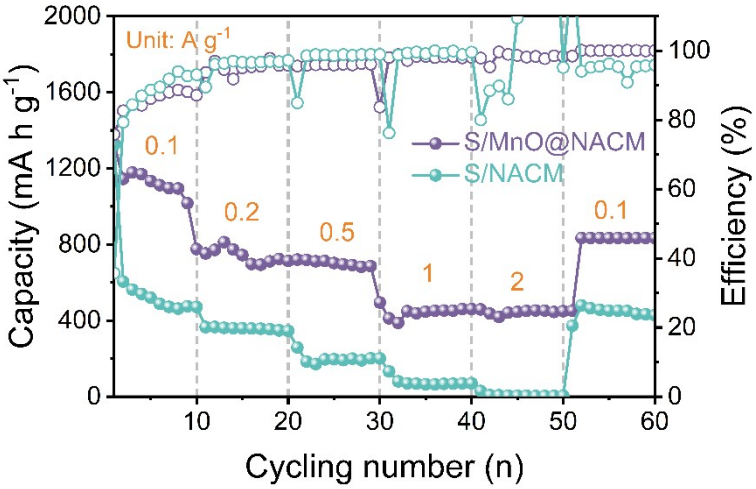

Figure S12. Rate performance of the Na-S coin cells at different current densities.

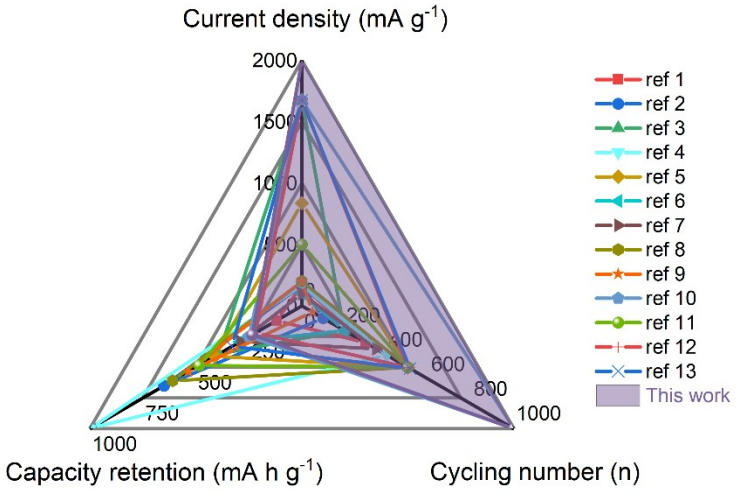

Figure S13. A comparison on cyclability of parts of S cathodes reported with this work.

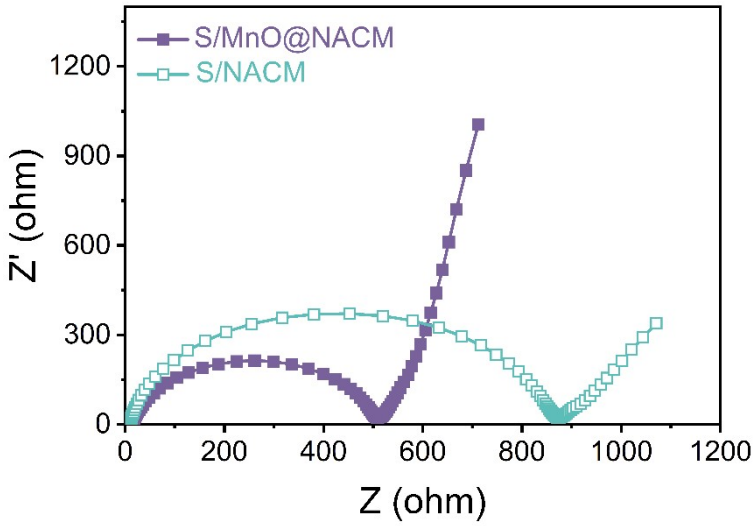

Figure S14. Nyquist plots of the S/MnO@NACM and S/NACM composite.

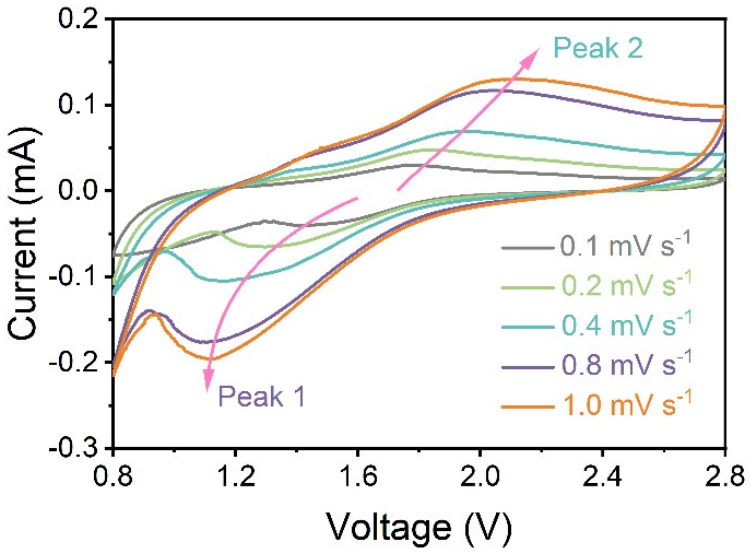

Figure S15. CV curves of the S/MnO@NACM composite at various scan rates from 0.1 mV s^{-1} to 1.0 mV s^{-1}.

References cited in Figure 3h:

[1] Q.Q. Lu, X.Y. Wang, J. Cao, C. Chen, K. Chen, Z.F. Zhao, Z.Q. Niu, J. Chen, Energy Storage Mater, 8 (2017) 77-84.

[2] Q.B. Guo, S. Li, X.J. Liu, H.C. Lu, X.Q. Chang, H.S. Zhang, X.H. Zhu, Q.Y. Xia, C.L. Yan, H. Xia, Adv Sci, 7 (2020) 1903246.

[3] L. Hu, Y. Lu, T.W. Zhang, T. Huang, Y.C. Zhu, Y.T. Qian, Acs Appl Mater Inter, 9 (2017) 13813-13818.

[4] Q. Guo , S. Sun , K. Kim , H. Zhang , X. Liu , C. Yan and H. Xia , Carbon Energy, 2 (2021) 1-9.

[5] T.T. Yang, W. Gao, B.S. Guo, R.M. Zhan, Q.J. Xu, H. He, S.J. Bao, X.Y. Li, Y.M. Chen, M.W. Xu, J Mater Chem A, 7 (2019) 150-156.

[6] Y.X. Wang, J.P. Yang, W.H. Lai, S.L. Chou, Q.F. Gu, H.K. Liu, D.Y. Zhao, S.X. Dou, J Am Chem Soc, 138 (2016) 16576-16579.

[7] L. Zhang, B.W. Zhang, Y.H. Dou, Y.X. Wang, M. Al-Mamun, X.L. Hu, H.K. Liu, Acs Appl Mater Inter, 10 (2018) 20422-20428.

[8] A. Kumar, A. Ghosh, A. Roy, M.R. Panda, M. Forsyth, D.R. MacFarlane, S. Mitra, Energy Storage Mater, 20 (2019) 196-202.

[9] A. Ghosh, A. Kumar, A. Roy, M.R. Panda, M. Kar, D.R. MacFarlane, S. Mitra, Acs Appl Mater Inter, 11 (2019) 14101-14109.

[10] T.T. Yang, B.S. Guo, W.Y. Du, M.K. Aslam, M.L. Tao, W. Zhong, Y.M. Chen, S.J. Bao, X. Zhang, M.W. Xu, Adv Sci, 6 (2019) 1901557.

[11] C.W. Dong, H.Y. Zhou, B. Jin, W. Gao, X.Y. Lang, J.C. Li, Q. Jiang, J Mater Chem A, 9 (2021) 3451-3463.

[12] L. Fan, R.F. Ma, Y.H. Yang, S.H. Chen, B.A. Lu, Nano Energy, 28 (2016) 304-310.

[13] Y. Liu, X.Y. Li, Y.Z. Sun, R. Yang, Y. Lee, J.H. Ahn, J Alloy Compd, 853 (2021) 157316.